2.4A *Kinematic, Microphysical and Lightning Properties of a Tornadic and Nontornadic Supercell during VORTEX-SE*

Austin D. Vacek, Lawrence D. Carey, Sarah M. Stough
University of Alabama in Huntsville, Huntsville, AL

1. INTRODUCTION

Tornadic supercell potential still remains a difficult challenge for forecasters, as only 26% of storms that experience a radar detected mesocyclone produce a tornado (Trapp et al. 2005). In order to better understand supercell processes related to severe weather, studies have implemented the use of total lightning and dual-polarization radar data.

Previous studies have shown that total lightning trends can be used as an indicator for severe weather occurrence (Goodman et al. 1988; Williams et al. 1999; Gatlin 2006; Schultz et al. 2009; Gatlin and Goodman 2010). Williams et al. (1999) observed rapid increases in total lightning, or lightning jumps, often occurred before a severe weather event. To quantify rapid total lightning increases, Schultz et al. (2009, 2011) developed a 2σ lightning jump algorithm to assist in nowcasting severe weather. Lightning jumps infer stronger updraft characteristics from an increase of mixed-phase graupel mass and peak maximum updraft speed, typically enhancing 4 to 13 minutes before lightning jump occurrence (Schultz et al. 2017). Rapid decreases in lightning rates have been observed before severe weather events in previous studies (Steiger et al. 2007), however studies lack examination of the importance it plays in storm development and processes. There are no known studies that examine lightning decreases with multi-Doppler and dual-polarization data.

Microphysical studies have shown differential reflectivity (Z_{DR}) can be used to diagnose storm severity and distinguish tornadic development potential. The presence of a Z_{DR} column indicates supercooled liquid drops are being elevated past the freezing level due to updraft vertical motions (Caylor and Illingworth 1987). Kumjian et al. (2014) found that Z_{DR} column height can be used as an indicator of updraft intensity. Other studies have examined Z_{DR} values associated with the supercell hook echo. Nontornadic supercells tend to have higher median Z_{DR} values within the hook echo compared to tornadic supercells, suggesting greater rates of evaporation may be occurring (Kumjian and Ryzhkov 2008; French et al. 2015). Tornadogenesis processes can be impacted due to the magnitude of evaporation rates in the rear-flank downdraft (RFD; Markowski et al. 2002).

The purpose of this study is to examine rapid decreases in total lightning trends, termed lightning dives, and microphysical properties between tornadic and nontornadic supercells during the Verification of the the Origins of Rotation in Tornadoes Experiment-Southeast (VORTEX-SE) field campaign. A detailed examination will investigate the role and correlation of lightning dives with storm vertical velocities, specifically in downdraft regions. In addition, Z_{DR} column heights and hook echo characteristics are compared with dual-Doppler vertical velocities. Therefore, the overall goal is to improve lead times and forecaster's confidence for severe weather threats during supercell events.

The lightning and radar data will be described in the next section, while section 3 provides the methodology implemented. Section 4 focuses on the lightning, kinematic, and microphysical properties experienced during the tornadic and nontornadic supercell evolution. Characterization and lightning trends are described in subsection 4.1, maximum vertical velocities are presented in subsection 4.2, followed by a microphysical examination of the Z_{DR} column and hook echo characteristics of the two supercells in subsection 4.3. A summary and future work outline are presented in section 5.

2. DATA

Two supercell cases of interest will be analyzed using lightning and radar data as they evolved within dual-Doppler lobes in the VORTEX-SE domain (Figure 1). On 31 March, 2016 (IOP3) a tornadic supercell produced an EF-2 tornado lasting 15 minutes. The other supercell was nontornadic, but developed low-level rotation and was tornado warned for 28 minutes on 30 April, 2016 (IOP6).

---

* C*orresponding author address:* Austin D. Vacek, Univ. of Alabama in Huntsville, Dept. of Atmospheric Sciences, Huntsville, AL 35816; e-mail: adv0005@uah.edu

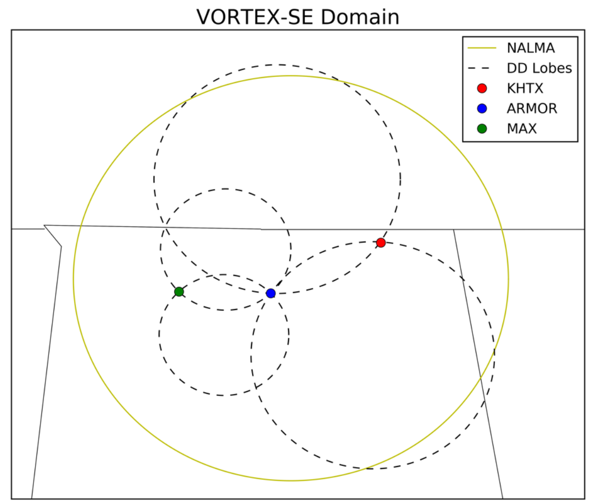

Figure 1: *VORTEX-SE domain with KHTX (red dot), ARMOR (blue dot), and MAX (green dot) locations. Black dashed lines are KHTX/ARMOR and ARMOR/MAX dual-Doppler lobes, and yellow line is the 125 km NALMA range ring.*

2.1 Lightning Data

Total lightning information is collected from NASA's North Alabama Lightning Mapping Array (NALMA) centered at the National Space Science and Technology Center on the University of Alabama in Hunstville (UAH) campus (Koshak et al. 2004; Goodman et al. 2005). NALMA consists of 11 station arrays measuring very high frequency (VHF) radiation source points from electrical breakdown, operating between 76 and 82 MHz. These VHF source points are collected and mapped in three dimensions every 80 μs. To construct a lightning flash, VHF source points are grouped using the McCaul et al. (2009) flash clustering algorithm. Each flash is required to have a minimum of 10 VHF source points to eliminate flashes constructed from noise. Lightning data are constrained to a 125 km range from the center of the NALMA as detection and accuracy begin to decrease from this range (Koshak et al. 2004).

2.2 Radar Data

The two supercells of interest are analyzed using a combination of the National Weather Service's (NWS) Weather Surveillance Radar 1988 Doppler (WSR-88D) S-band radar located at Hytop, Alabama (KHTX; Crum and Alberty 1993), the UAH's Advanced Radar for Operational Research (ARMOR; Peterson et al. 2005) C-band radar located at Huntsville International Airport, and Mobile Alabama X-band (MAX) radar located at Courtland Airport. Next Generation Weather Radar (NEXRAD) Level II format data were acquired from National Oceanic and Atmospheric Administration's (NOAA) National Climatic Data Center (NCDC) archive to track supercell coordinate locations. The radar baseline distance between KHTX and ARMOR (ARMOR and MAX) is 70 km (53 km).

3. METHODOLOGY

3.1 Lightning Tracking and Dive

Storm locations are determined by merging WSR-88D radar reflectivity in NOAA National Severe Storms Laboratory (NSSL) Warning Decision Support System – Integrated Information (WDSS-II; Lakshmanan et al. 2007). Merged reflectivity is outputted in two minute intervals and the low-level maximum reflectivity coordinate of the supercell is extracted. The latitude and longitude coordinate is then expanded using a subjective bounding box radius to isolate lightning activity from other storms.

Once lighting flashes have been identified to a supercell, a similar algorithm to Schultz et al. (2009, 2011) is implemented to identify +2σ lightning jumps and -2σ lightning dives. Sigma levels are computed from the ratio of the current time rate of change of the total flash rate (DFRDT) and the standard deviation of the previous five DFRDT values. A -2σ (+2σ) lightning dive (jump) is classified as when the current DFRDT exceeds twice the negative (positive) standard deviation of the previous five DFRDT values. Flash rates must be greater than 10 flashes min^{-1} to activate either a lightning jump or lightning dive, and only one is counted between a six minute period.

3.2 Dual-Doppler Analysis

Doppler radial velocities are dealiased using the National Center for Atmospheric Research's (NCAR) SOLO, version 3 software (Oye et al. 1995). Ground clutter and sidelobes are also removed during this step. Radar data are then gridded onto a Cartesian coordinate system with a Cressman weighting scheme using a 1 km X 1 km X 0.5 km (X, Y, Z) grid spacing on an 80 km X 80 km X 15 km grid. Dual-Doppler wind synthesis is performed using NCAR's Custom Editing and Display of Reduced Information in Cartesian Space (CEDRIC; Mohr et al. 1986). Maximum vertical velocities are retrieved by a downward integration of the mass continuity equation with an upper boundary condition of vertical motion set to 0 m s^{-1}. Downward integration is a more accurate approach when vertically topping the supercell of interest (O'Brien 1970; Ray et al. 1980; Matejka and Bartles 1998). Bulk hydrometeor terminal fall speed estimates are found using a linear reflectivity relationship when calculating vertical motions (Marks and Houze 1987). Radar volumes between the two radars were required to be within two minutes of each other to ensure accurate vertical velocity retrieval.

3.3 *Microphysical Analysis*

All dual-polarization signatures are evaluated using ARMOR for continuity between the two cases and close proximity to each supercell. The dual-polarization Z_{DR} column feature will be examined during the evolution of each supercell. After gridding the radar data, the height of the 1 dB contour above the melting level is recorded. Updraft intensity will be examined and correlated with the height of the Z_{DR} column.

When analyzing hook echo characteristics, the lowest elevation scan not subjected to noise is used from ARMOR. Rather than using gridded data, the hook echo Z_{DR} pixel values are incorporated for a more accurate representation of hydrometeors. Pixels must meet a radar reflectivity factor ≥ 35 dBZ and a cross-correlation coefficient ≥ 0.85 threshold to ensure ground clutter and non-hydrometeors are not measured. Median Z_{DR} hook echo values are tracked during the evolution of each supercell and then compared to RFD velocities.

4. RESULTS

To investigate the role of lightning dives, a tornadic and nontornadic supercell are examined. Lightning trends of each supercell are described in the next subsection, followed by vertical velocities associated with lightning jump and lightning dive occurrence, concluding with an intercomparison of vertical velocities with microphysical properties and processes.

4.1 *Lightning Trends*

Lightning flash rates remained fairly low, maximum of 27 flashes minute^{-1}, throughout the lifespan of the tornadic supercell (Figure 2). At 0141 UTC, a lightning jump was produced 16 minutes before tornado formation (0157 UTC). After the rapid increase in lightning, a drastic decrease in flash rates occurred producing a lightning dive eight minutes after (0149 UTC) the lightning jump.

The nontornadic supercell experienced higher flash rates with a cyclic nature during its evolution (Figure 3). The tornado warning period was between 2132 UTC and 2200 UTC, with a 50-60 mph damaging wind report at 2200 UTC. A lightning jump was produced at 2142 UTC, followed by a lightning dive at 2204 UTC. Analysis will examine the role of the first lightning jump and lightning dive that occurred during the tornado warning period.

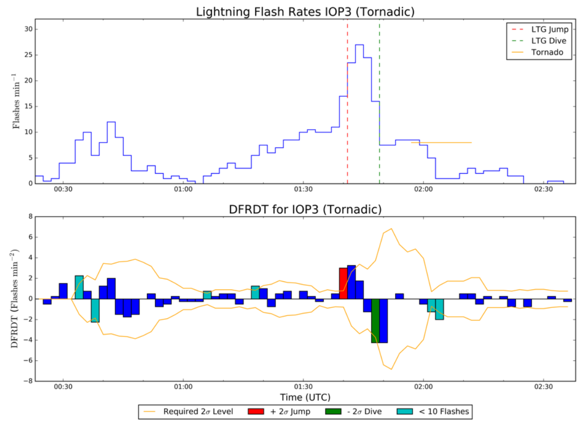

Figure 2: *Two minute averaged lightning trends experienced throughout the lifespan of the tornadic supercell (top). Red dashed lines are lightning jumps, green dashed lines are lightning dives, and the orange line is the duration of the tornado. Running DRFDT and (+/-) 2σ level required for a lightning jump or dive to be triggered (bottom). Orange line is the positive and negative 2σ level, red boxes are lightning jumps, green boxes are lightning dives, and cyan boxes are jumps or dives not meeting the 10 flash requirement.*

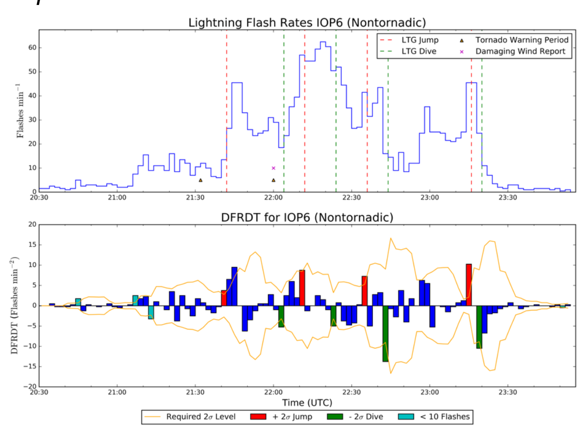

Figure 3: *Nontornadic supercell lightning trends. Same as Figure 2, however pink cross denotes a damaging wind report.*

4.2 *Vertical Velocities*

Magnitudes of the vertical velocities are distinctively different between the two supercells. Maximum vertical velocities are separated by updraft, forward-flank downdraft (FFD), and RFD

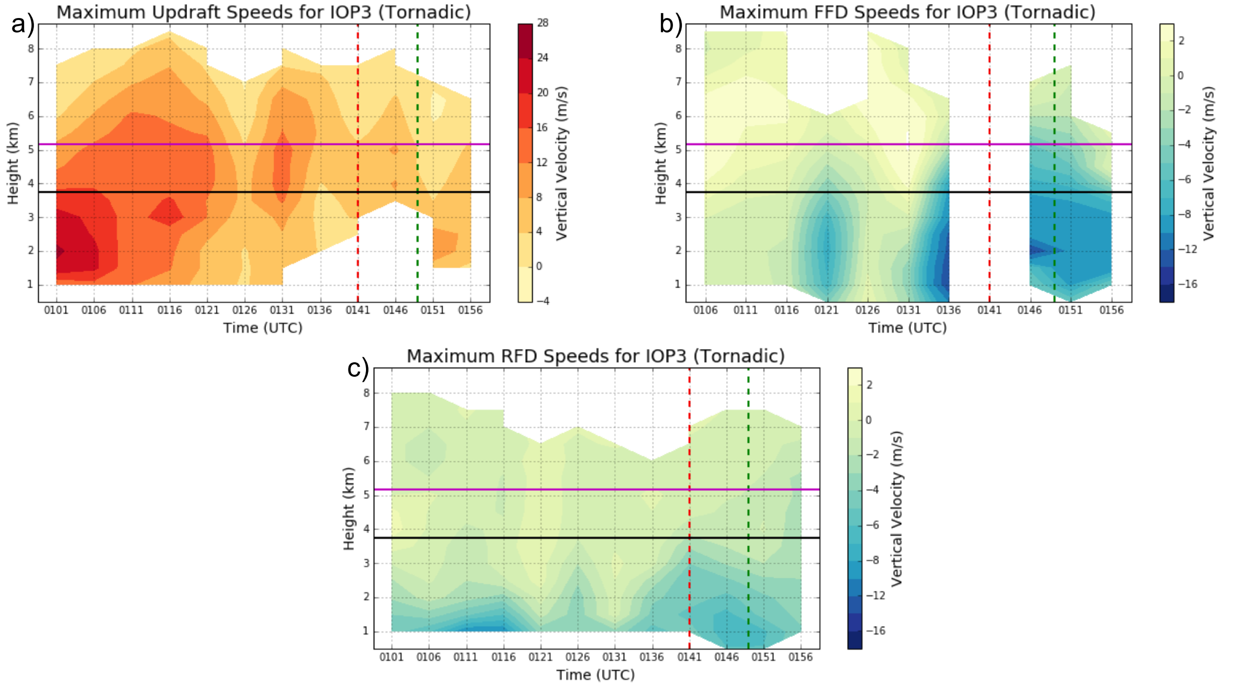

Figure 4: *Tornadic supercell maximum vertical velocity time height plots. Maximum updraft vertical velocity (a), maximum forward-flank downdraft vertical velocity (b), maximum rear-flank downdraft vertical velocity (c), lightning jump occurrence (dashed red line), lightning dive occurrence (dashed green line), 0 °C height (solid black line), -10 °C height (solid purple line).*

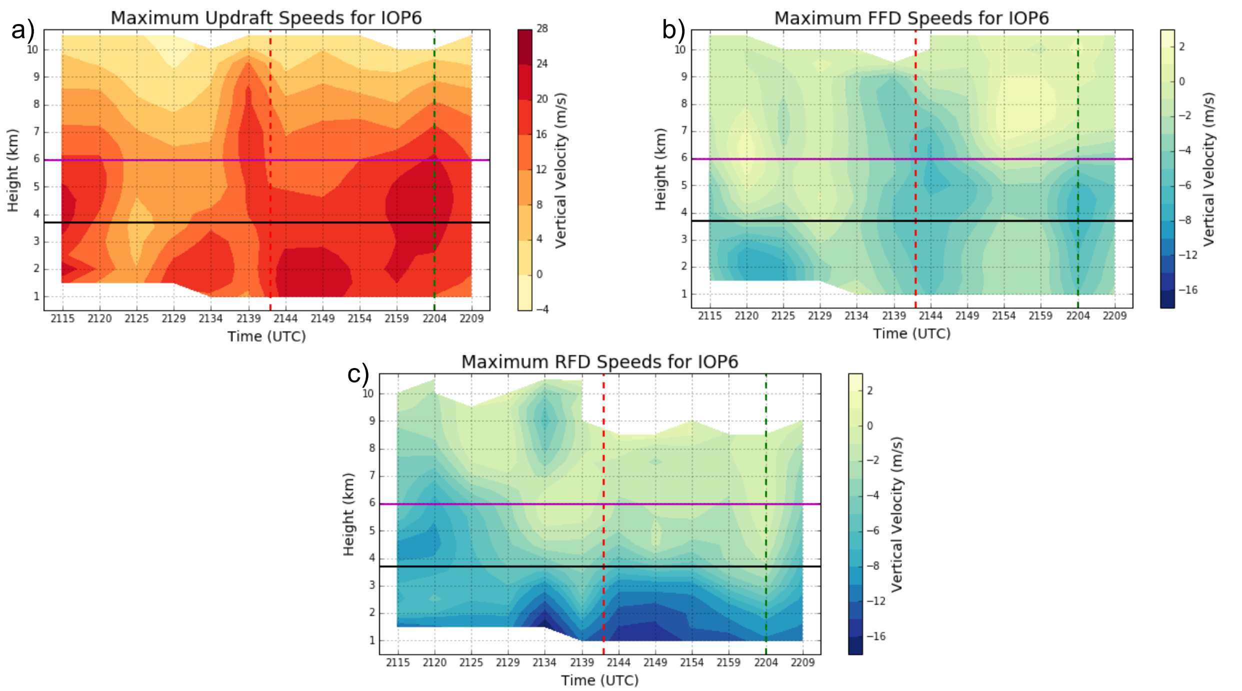

Figure 5: *Nontornadic supercell maximum vertical velocity time height plots. Same setup as Figure 4.*

regions for the tornadic supercell in Figure 4. Noticeably larger updraft speeds occur at the beginning of the supercell evolution (Figure 4a). However, the maximum updraft speeds decrease at 0126 UTC, when the supercell became cyclic. A mixed-phase updraft enhancement occurs 10 minutes prior to the lightning jump, then maximum updraft speeds decrease around 8 m s^{-1} leading to tornado formation. Low-level MAX attenuation issues in the inflow notch of the supercell cause missing updraft velocities starting at 0136 UTC. The FFD experienced an enhancement at low-levels (~14 m s^{-1}) beginning at 0136 UTC and 13 minutes before the lightning dive (Figure 4b). Enhanced FFD values persist for the duration leading to tornadogenesis. At 0141 UTC, a missing FFD signature occurs due to attenuation issues and storm topping in the vertical becomes limited. Small downward vertical motions are present throughout the duration of the RFD (Figure 4c). A slight low-level enhancement occurs at 0146 UTC (~7 m s^{-1}), three minutes before the lightning dive and 11 minutes before tornado formation.

Nontornadic supercell maximum vertical velocities are presented in Figure 5. Maximum updraft speeds are consistently larger, peaking at 22 m s^{-1}, during the tornado warning period than compared to the tornadic supercell (Figure 5a). Three minutes before the lightning jump, a mixed-phase updraft enhancement occurs at 2139 UTC. The FFD possessed overall smaller downward vertical motions, with an enhancement (~7 m s^{-1}) occurring simultaneous to the lightning dive (2204 UTC; Figure 5b). Downward vertical motions are the largest in the RFD, with a low-level enhancement (15 m s^{-1}) 20 minutes before the lightning dive and 16 minutes before the damaging wind report (Figure 5c).

4.3 *Dual-Polarization Signatures*

A time series plot of Z_{DR} column heights is presented to describe the differences of evolution between the two supercells and compare dual-Doppler retrieved updraft vertical velocities (Figure 6). The tornadic supercell experienced maximum Z_{DR} column heights prior to the storm becoming cyclic, correlating to the largest updraft velocities during the supercell lifespan. Heights of the Z_{DR} column begin to decrease during the cyclic period, however a peak occurs at 0131 UTC matching the time of the mixed-phase updraft enhancement. Heights continue to diminish leading to tornadogenesis with multiple radar volumes not experiencing a 1 dB contour above the freezing level. As previously mentioned, the nontornadic supercell sustained

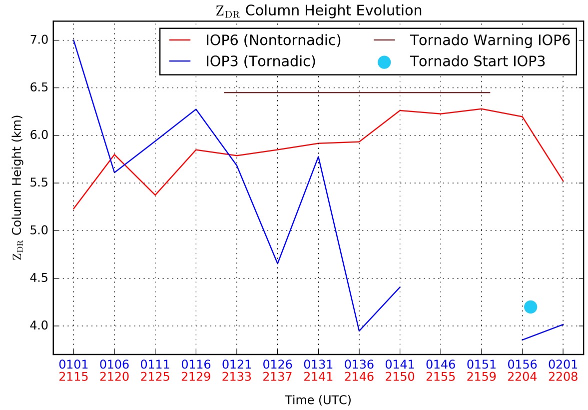

Figure 6: *Evolution of Z_{DR} column height for the tornadic supercell (blue line) and the nontornadic supercell (red line). Tornado start period (light blue circle) and the tornado warning period are identified (brown line).*

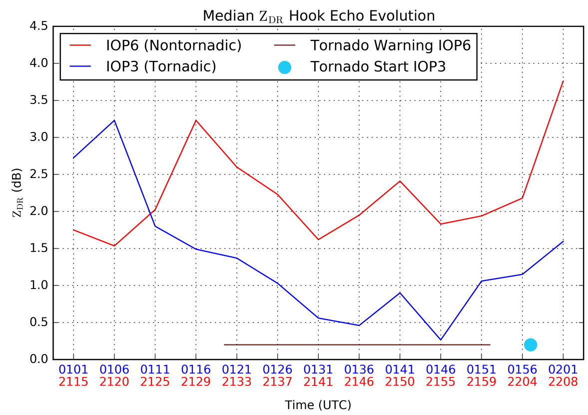

Figure 7: *Evolution of median Z_{DR} values within the hook echo for the tornadic supercell (blue line) and the nontornadic supercell (red line). Tornado start period and the tornado warning period are identified as in Figure 6.*

larger maximum updraft velocities during the tornado warning period than the tornadic supercell period leading to tornadogenesis. This is evident in the Z_{DR} column heights remaining around 6.0 km during the tornado warning period, whereas the tornadic supercell Z_{DR} column signature was faintly present. This portrays confidence in maximum updraft velocities retrieved from dual-Doppler analysis.

Median Z_{DR} pixel hook echo values are then compared to maximum RFD velocities for the tornadic and nontornadic supercell (Figure 7). Starting with the tornadic supercell, median Z_{DR} pixel values hovered around 0.78 dB in the radar volumes 30 minutes prior to tornado formation. The nontornadic supercell hook echo median Z_{dr} pixel values were significantly larger (~2.09 dB) during the tornado warning period. This suggests larger Z_{DR}-inferred drops are occurring in the nontornadic supercell hook echo. As suggested by Kumjian and Ryzhkov (2008), larger median Z_{DR} hook echo values may be due to greater evaporation rates depleting smaller drops. Evaporation rates and larger drops may lead to greater terminal fall speeds, which is in agreement with the dual-Doppler wind retrieval of greater maximum RFD values for the nontornadic supercell.

5. SUMMARY & FUTURE WORK

This study quantifies rapid decreases in lightning using a -2σ lightning dive approach and the role it may play in vertical motions. To understand kinematic and microphysical processes, the evolution of a tornadic and nontornadic supercell within dual-Doppler lobes are analyzed.

In both supercell cases, a lightning dive occurred 13 (0) minutes after a FFD enhancement and 3 (20) minutes after a RFD enhancement for the tornadic (nontornadic) supercell. A lightning jump proceeded a mixed-phase updraft enhancement by 3 and 10 minutes, in general agreement with Schultz et al. (2017). Lightning trends can play a valuable role in forecasting supercell evolution.

Vertical motion magnitudes could have played a large role in tornadogenesis maintenance or failure. Lemon and Doswell (1979) suggested tornado formation is dependent upon the mesocyclone becoming divided between an intense updraft beginning to weaken in magnitude and the RFD intensifying. This “Goldilocks Zone” scenario appears plausible for the tornadic supercell after the updraft weakens and an enhancement of the RFD starts 11 minutes before tornadogenesis. The nontornadic supercell experienced consistently larger updraft and RFD magnitudes, possibly the cause of tornadogenesis failure.

Larger evaporation rates may be present in the nontornadic supercell, leading to larger Z_{DR}-inferred drops in the hook echo. This is a consistent finding also noted in Kumjian and Ryzhkov (2008) and French et al. (2015). The RFD magnitudes may be influenced by evaporation rates as well as drop size distribution terminal fall speeds.

Despite a small case sample, both the tornadic and nontornadic supercells showed utility of a lightning dive. We do note that not all supercells experience a lightning dive or even a decrease in lightning before a severe weather event. The presence of a lightning dive may give forecasters the added confidence to issue a severe weather threat due to an enhancing downdraft. Future work will consist of adding more cases from the 2016 VORTEX-SE database, as well as adding 2017 VORTEX-SE cases that are applicable.

Acknowledgements:
This material is based upon work supported by NOAA/OAR/NSSL and the VORTEX-SE program within NOAA/OAR Office of Weather and Air Quality under Grant No. NA15OAR4590230.

6. REFERENCES

Caylor, I. J., and A. J. Illingworth, 1987: Radar observations and modeling of warm rain initiation. *Quart. J. Roy. Meteor. Soc.*, 113, 1171-1191, doi: 10.1002/qj.49711347806.

Crum, T. D., and R. L. Alberty, 1993: The WSR-88D and the WSR-88D Operational Support Facility. *Bull. Amer. Meteor. Soc.*, **74**, 1669-1687.

French, M. M., D. W. Burgess, E. R. Mansell, and L. J. Wicker, 2015: Bulk hook echo raindrop sizes retrieved using mobile, polarimetric Doppler radar observations. *J. Appl. Meteor. Climatol.*, **54**, 423-450, doi: 10.1175/JAMC-D-14-0171.1.

Gatlin, P., 2006: Severe weather precursors in the lightning activity of Tennessee Valley thunderstorms. M.S. thesis, The University of Alabama in Huntsville.

Gatlin, P., and S. J. Goodman, 2010: A total lightning trending algorithm to identify severe thunderstorms. *J. Atmos. Oceanic Technol.*, **27**, 3-22, doi: 10.1175/2009JTECHA1286.1.

Goodman, S. J., D. E. Buechler, P. D. Wright, and W. D. Rust, 1988: Lightning and precipitation history of a microburst-producing storm. *Geophys. Res. Lett.*, **15**, 1185–1188.

Goodman, S. J., and Coauthors, 2005: The North Alabama Lightning Mapping Array: Recent severe storm observations and future prospects. *Atmos. Res.*, **76**, 423–437.

Koshak, W. J., and Coauthors, 2004: North Alabama Lightning Mapping Array (LMA): VHF source retrieval algorithm and error analysis. *J. Atmos. Oceanic Technol.*, **21**, 543–558.

Kumjian, M. R., A. P. Khain, N. BenMoshe, E. Ilotoviz, A. V. Ryzhkov, and V. T. J. Phillips, 2014: The anatomy and physics of Z_{dr} columns: Investigating a polarimetric radar signature with a spectral bin microphysical model. *J. Appl. Meteor. Climatol.*, **53**, 1820-1843.

Kumjian, M. R., A. V. Ryzhkov, 2008: Microphysical differences between tornadic and non-tornadic supercell rear-flank downdrafts revealed by dual-polarization radar measurements. Preprints, *24th Conf. on Severe Local Storms*, Savannah, GA, Amer. Meteor. Soc., 3B.4.

Lakshmanan, V., T. Smith, G. Stumpf, and K. Hondl, 2007: The warning decision support system-integrated information. *Weather Forecast*., **22**, 596-612, doi: 10.1175/WAF1009.1.

Lemon, L. R., and C. A. Doswell III, 1979: Severe thunderstorm evolution and mesocyclone structure as related to tornadogenesis. *Mon. Wea. Rev.*, **107,** 1184–1197.

Markowski, P. M., J. M. Straka, and E. N. Rasmussen, 2002: Direct surface thermodynamic observations within the rear-flank downdrafts of nontornadic and tornadic supercells. *Mon. Wea. Rev.*, **130**, 1692-1721.

Marks, F. D., and R. A. Houze Jr., 1987: Inner core structure of Hurricane Alicia from airborne Doppler radar observations. *J. Atmos. Sci.*, **44**, 1296-1317.

Matejka, T., and D. L. Bartels, 1998: The accuracy of vertical air velocities from Doppler radar data. *Mon. Wea. Rev.*, **126**, 92-117, doi: 10.1175/1520-0493(1998)126<0092:TAOVAV>2.0.CO;2.

McCaul, E. W., S. J. Goodman, K. M. LaCasse, and D. J. Cecil, 2009: Forecasting lightning threat using cloud-resolving model simulations. *Wea. Forecasting*, **24**, 709-729.

Mohr, C. G., L. J. Miller, R. L. Baughan, and H. W. Frank, 1986: Merger of mesoscale data sets into a common Cartesian format for efficient and systematic analysis. *J. Atmos. Oceanic Technol.*, **3**, 143-161.

O'Brien, J. J., 1970: Alternative solutions to the classical vertical velocity problem. *J. Appl. Meteor.*, **9**, 197-203.

Oye, D., C. Mueller, and S. Smith, 1995: Software for radar translation, visualization, editing and interpolation. Preprints, *27th Conf. on Radar Meteorology*, Vail, CO, Amer. Meteor. Soc., 359-361.

Petersen W. A., and Coauthors, 2005: The UAH-NSSTC/WHNT ARMOR C-band dual-polarimetric radar: A unique collaboration in research, education and technology transfer. Preprints, *32nd Conf. on Radar Meteorology,* Albuquerque, NM, Amer. Meteor. Soc.

Ray, P. S., C. L. Ziegler, W. B. Bumgarner, and R. J. Serafin, 1980: Single- and multiple-Doppler radar observation of tornadic storms. *Mon. Wea. Rev.*, **108**, 1607-1625.

Schultz, C. J., W. A. Petersen, and L. D. Carey, 2009: Preliminary development and evaluation of lightning jump algorithms for the real-time detection of severe weather. *J. Appl. Meteor. Climatol.*, **48**, 2543–2563. doi: 10.1175/2009JAMC2237.1

Schultz, C. J., W. A. Petersen, L. D. Carey, 2011: Lightning and severe weather: A comparison between total and cloud-to-ground lightning trends. *Wea. Forecasting*, **26**, 744-755. doi: 10.1175/WAF-D-10-05026.1

Schultz, C. J., L. D. Carey, E. V. Schultz, R. J. Blakeslee, 2017: Kinematic and microphysical significance of lightning jumps versus nonjump increases in total flash rate. *Wea. Forecasting*, **32**, 275-288.

Steiger, S. M., R. E. Orville, and L. D. Carey, 2006: Total lightning signatures of thunderstorms intensity over North Texas. Part I: Supercells. *Mon. Wea. Rev.*, **135**, 3281-3302.

Trapp, R. J., G. J. Stumpf, and K. L. Manross, 2005: A reassessment of the percentage of tornadic mesocyclones. *Wea. Forecasting*, **20**, 680–687.

Williams, E. R., and Coauthors, 1999: The behavior of total lightning activity in severe Florida thunderstorms. *Atmos. Res.*, **51**, 245–265.